Transfection of the CD20 Cell Surface Molecule into Ectopic Cell Types Generates a Ca^{2+} Conductance Found Constitutively in B Lymphocytes

James K. Bubien,* Liang-Ji Zhou,§ P. Darwin Bell,‡ Raymond A. Frizzell,‡ and Thomas F. Tedder§

*Departments of Medicine and ‡Physiology and Biophysics, University of Alabama at Birmingham, Birmingham, Alabama 35294; and §Division of Tumor Immunology, Dana-Farber Cancer Institute, and Department of Pathology, Harvard Medical School, Boston, Massachusetts 02115-6084

Abstract. CD20 is a plasma membrane phosphoprotein expressed exclusively by B lymphocytes. mAb binding to CD20 alters cell cycle progression and differentiation, indicating that CD20 plays an essential role in B lymphocyte function. Whole-cell patch clamp and fluorescence microscopy measurements of plasma membrane ionic conductance and cytosolic-free Ca^{2+} activity, respectively, were used to directly examine CD20 function. Transfection of human T and mouse pre-B lymphoblastoid cell lines with CD20 cDNA and subsequent stable expression of CD20 specifically increased transmembrane Ca^{2+} conductance. Transfection of CD20 cDNA and subsequent expression of CD20 in nonlymphoid cells (human K562 erythroleukemia cells and mouse NIH-3T3 fibroblasts) also induced the expression of an identical transmembrane Ca^{2+} conductance. The binding of a CD20-specific mAb to $CD20^+$ lymphoblastoid cells also enhanced the transmembrane Ca^{2+} conductance. The mAb-enhanced Ca^{2+} currents had the same conductance characteristics as the CD20-associated Ca^{2+} currents in CD20 cDNA-transfected cells. C20 is structurally similar to several ion channels; each CD20 monomer possesses four membrane spanning domains, and both the amino and carboxy termini reside within the cytoplasm. Biochemical cross-linking of cell-surface molecules with subsequent immunoprecipitation analysis of CD20 suggests that CD20 may be present as a multimeric oligomer within the membrane, as occurs with several known membrane channels. Taken together, these findings indicate that CD20 directly regulates transmembrane Ca^{2+} conductance in B lymphocytes, and suggest that multimeric complexes of CD20 may form Ca^{2+} conductive ion channels in the plasma membrane of B lymphoid cells.

CD20 was among the first lineage-specific differentiation antigens to be identified on human B lymphocytes, after surface Ig (43). CD20 is found on the cell surface of early B cell precursors and all mature B cells, and it is lost with differentiation into plasma cells (33, 38, 43, 44). The specific function of CD20 has not been previously elucidated, however, CD20 function has been associated with cell cycle progression. mAb binding to CD20 inhibits B lymphocyte progression into the S/G2+M stages of cell cycle following mitogen stimulation (15, 50, 51), and also inhibits B lymphocyte differentiation and Epstein-Barr virus- and pokeweed mitogen-induced Ig secretion (15, 19, 20, 50, 51). Additionally, one CD20 mAb (1F5) that binds to a unique CD20 epitope (10, 48) is capable of activating dense tonsilar (G_o) B lymphocytes (10, 20, 40). CD20 is not phosphorylated in resting B cells, but becomes heavily phosphorylated after mitogen stimulation, providing further evidence that CD20 is involved in B cell activation and differentiation (47, 57). CD20 is a dominant phosphoprotein in activated B cells, B cell lines, and Hairy cell leukemias (17, 47). In addition, mAb binding to CD20 generates a transmembrane signal that results in enhanced phosphorylation of the molecule (47), initiation of tyrosine-kinase activity (26) and induction of *c-myc* oncogene expression (40). The effects of mAb binding are thought to be consequences of altered CD20 function and therefore indicate that CD20 plays a role in B lymphocyte activation, proliferation, and differentiation.

CD20 is a structurally unique protein that contains three extensive hydrophobic regions of sufficient lengths to pass through the membrane four times (13, 42, 52, 54). The long carboxy- and amino-terminal ends of the molecule are located within the cytoplasm with only a minor portion of the molecule exposed to the extracellular environment. The transmembrane and cytoplasmic regions of both mouse and human CD20 are well conserved and may allow for interactions with multiple proteins that are co-immunoprecipitated with CD20 (35, 53). Three forms of CD20 (33,000, 35,000, and 37,000 M_r) result from differential phosphorylation of a single protein species at different serine and threonine residues within the cytoplasmic domains (47, 53). PMA

treatment of B cells causes a reduction of the 33,000-M_r form and a proportional increase in the amount of the 35,000–37,000-M_r forms (47), suggesting that phosphorylation may be one molecular mechanism which regulates CD20 function (47, 57).

CD20 shares a common chromosomal location, and a similar overall structure and sequence homologies with the β chain of the high affinity IgE receptor (FcϵRI) found on mast cells and basophilic leukemia cells (25, 52, 55). This suggests that CD20 and the FcϵRI β chain are members of a single gene family. Although, IgE-mediated degranulation of mast cells does not appear to require opening of ion channels (32), the FcϵRI complex has long been associated with plasma membrane Ca^{2+} conductance, because antigenic cross-linking of receptors induces a transient increase in cytosolic-free Ca^{2+} (58) which is associated with a net influx of Ca^{2+} into the cells probably through Ca^{2+} channels (32, 37). Reconstitution of the FcϵRI complex into lipid bilayers produced Ca^{2+} channel activity and suggests that the β subunit may constitute the pore-forming component of the receptor complex (11). The predicted structure of CD20 suggests that it may also function as a channel, since multiple membrane-spanning domains and phosphorylation sites on the cytoplasmic domains are hallmarks of ligand-gated ion channels and other channel forming molecules (30, 60). The sequence homology within the transmembrane domains of CD20 and FcϵRI β chain suggest that these proteins may represent a unique family of proteins which function either directly as ligand-gated ion channels or as essential components of such channels.

The expression of CD20 in heterologous cells transfected with CD20 cDNA allowed us to directly test the hypothesis that CD20 mediates a plasma membrane ionic conductance in B lymphocytes. Minimally, the findings demonstrate that CD20 plays a direct role in the regulation of transmembrane conductive Ca^{2+} flux, which elucidates a function for CD20 and provides a mechanistic explanation for the role of CD20 as a regulator of B lymphocyte activation and proliferation. The findings also support the hypothesis that CD20 is itself a Ca^{2+} channel, but they do not rule out the possibility that CD20 may be an essential regulatory element in a heterologous oligomer complex which functions as an ion channel.

Materials and Methods

CD20 cDNA Transfection of Cell Lines

The human CD20 cDNA clone pB1-21 (54) was cloned into the BamHI site of the retroviral vector pZipNeoSV(X) (8) so that the 5′ end of the cDNA coincided with that of the transcripts originating from the promoter in the long terminal repeat. This plasmid was named pZip.HuB1. Cell lines which do not endogenously express CD20 (Jurkat, Rex, 300.19, K562, and NIH-3T3 cells) were grown in RPMI 1640 medium (GIBCO BRL, Gaithersburg, MD) supplemented with 10% FCS (Hyclone Labs, Logan, UT), 2 mM L-glutamine, 50 U/ml penicillin, and 50 μg/ml streptomycin. Cells from each line were transfected with the pZipNeoSV(X) vector alone (controls) or pZip.HuB1 using the Cell-Porator Electroporation system (Bethesda Research Laboratories, Gaithersburg, MD). The parameters for electroporation were: 100 μg of plasmid DNA per 5×10^6 cells in 0.5 ml of DME medium (GIBCO BRL) on ice, 1.6 millifarads, 250 V/0.4 cm, using the high ohm setting. Transfected cells were selected for using medium with 1 mg/ml Geneticin (GIBCO BRL) added. Jurkat clones expressing CD20 (Jurkat-CD20) were isolated by limiting dilution of the cell population. CD20 positive Rex (Rex-CD20), 300.19 (300.19-CD20), K562 (K562-CD20), and NIH-3T3 (NIH-3T3-CD20) transfected cells were isolated by panning on culture dishes coated with the anti-Bla (CD20) mAb, and therefore were oligoclonal. In all cases $\geq$95% of the cells were $CD20^+$ as determined by indirect immunofluorescence staining with flow cytometry analysis. The surface antigen phenotypes of the transfected human cells were examined using mAb reactive with surface Ig, class I and class II major histocompatibility antigens, CD2, CD3, CD4, CD8, CD15, CD19, CD20, CD21, CD24, CDw29, CD38, CD40, CD45, CD45RA, and CD56. The mouse pre-B cell line 300.19 was examined for surface Ig and human CD20 expression.

Antibodies and Flow Cytometry Analysis

The CD20 mAb used in these studies were the anti-Bla (IgG2a) mAb (provided by Dr. Lee Nadler, Dana-Farber Cancer Institute, Boston, MA) as described (43), and the 1F5 mAb (IgG2a) mAb (provided by Dr. Edward Clark, Seattle University, Seattle, WA) as described (10). The CD21-specific mAb, HB-5 (IgG2a) was as described (49). The anti-Bla and HB-5 mAb were purified by salt precipitation followed by anion-exchange chromatography. The 1F5 mAb was purified by protein A affinity chromatography. All of the mAb were used in PBS. The anti-MHC class I mAb, W6/32, was used as ascites fluid (3).

Indirect immunofluorescence analysis was carried out after washing the cells three times. Suspensions of viable cells were analyzed for surface antigen expression by incubation for 20 min on ice with the appropriate mAb as ascites fluid diluted to the optimal concentration for immunostaining. After washing, the cells were treated for 20 min at 4°C with FITC-conjugated goat anti-mouse Ig antibodies (Southern Biotechnology Associates, Birmingham, AL). Single color immunofluorescence analysis was performed on an Epics Profile flow cytometer (Coulter Electronics, Hialeah, FL). 10,000 cells were analyzed in each instance and all histograms are shown on a three-decade log scale.

The average number of CD20 molecules present on the surface of parental Daudi cells was estimated by determining the number of anti-B1 mAb binding sites by Scatchard analysis (39). Cells were incubated for 60 min at 4°C with sub-saturating amounts of ^{125}I-labeled anti-B1 mAb in PBS. The cells were then layered on a 750-μl cushion of 75% (vol/vol) calf serum and centrifuged. The cell pellet was isolated and bound ^{125}I assessed by gamma counting. The specific activity of labeled mAb was determined by self-displacement curve analysis (7). The approximate number of CD20 molecules present on the surface of transfected cells was determined by flow cytometry analysis using Daudi cells as a standard. Cells were treated with saturating concentrations of FITC-conjugated anti-B1 mAb (Coulter Immunology, Hialeah, FL) and the mean channel of fluorescence staining determined by flow cytometry analysis using a linear scale. Approximate values for numbers of CD20 molecules were determined by extrapolation from values obtained with Daudi cells.

Biochemical Analysis

Cells were washed twice, resuspended in saline, and surface labeled by lactoperoxidase-catalyzed iodination as described (18). Alternatively, the cells (10^7 cells/ml) were metabolically labeled by culturing them for 90 min in medium containing [^{32}P]orthophosphate (125 μCi/ml) after culture in phosphate-deficient medium for 60 min as described (47). In some experiments, PMA (100 ng/ml; Sigma Immunochemicals, St. Louis, MO) was added to the cultures during the last 15 min of labeling. After labeling, the cells were washed twice and lysed in 1 ml of buffer containing 1% (vol/vol) Triton X-100 and protease inhibitors as described (47, 53). Immunoprecipitations were carried out using anti-Bla mAb and protein A–coated Sepharose beads (Pharmacia-LKB, Piscataway, NJ). The cell lysates were first precleared twice for 2 h using 2 μl of ascites fluid containing an unreactive IgG2a mAb and 50 μl (50% vol/vol) protein A-Sepharose at 4°C. The precleared lysate was then divided into equal samples and incubated with 2 μl of anti-Bla mAb and 50 μl of protein A beads (50% vol/vol) or murine IgG and beads with constant rotation at 4°C for 18 h. Immunoprecipitates were washed and analyzed by SDS-PAGE as described (47, 53) with subsequent autoradiography. Relative molecular weights were determined using pre-stained standard molecular weight markers (GIBCO BRL).

Chemical Cross-linking of Cell Surface Molecules

B lymphoblastoid cells (BJAB; 2×10^6/ml) were surface labeled by lactoperoxidase-catalyzed iodination, suspended in cold PBS (pH 7.0) and kept on ice. Dithio*bis*(succinimidylpropionate) (DSP)[1] (Pierce Chemical

1. *Abbreviations used in this paper*: CRAC, calcium release-activated calcium, DSP, dithiobis(succinimidylpropionate); NMDG, *N*-methyl-D-glucamine.

Co., Arlington Heights, IL) was used to crosslink the plasma membrane proteins. DSP was dissolved in DMSO (10 mg/ml) and added to the cell pellet at a final concentration of 10 μg in 1 ml. The cross-linking reaction was allowed to proceed for 50 min while kept on ice to reduce the fluidity of the plasma membranes. After this treatment, the cells were washed twice with cold PBS and lysed in buffer containing 0.5% NP-40, and 1% (wt/vol) BSA as described (47). CD20 was first precipitated from the detergent-solubilized material, followed by MHC class 1 antigen using W6/32 antibody as described (47). BSA was included in excess in all lysis and wash buffers to prevent further cross-linking of the solubilized membrane proteins. Immunoprecipitated proteins were divided and electrophoresed in the presence of SDS on a 10% acrylamide gel. One lane of the gel was fixed and dried for autoradiography. The other lane was soaked in an SDS solution containing mercaptoethanol (5%) for 2 h, laid on top of another 10% acrylamide slab gel, electrophoresed under reducing conditions, and autoradiographed. All autoradiographs were exposed for 5 d, except the MHC class I immunoprecipitations, which were only exposed overnight.

Whole-Cell Patch-Clamp Analysis

All transfected cells were cultured in RPMI 1640 with 10% FBS added. All cells were kept at 37°C in 95% CO_2 and the cell density was maintained at ~10^6 cell/ml. Immediately before use, the cells were washed twice in serum-free RPMI 1640, and placed in a perfusion chamber mounted on the stage of a Nikon diaphot inverted microscope. All electrophysiological experiments were performed at room temperature (24 ± 2°C).

High-resistance seals (10–100 Gohms) between micropipettes (0.5–1 micron i.d.) and individual cell plasma membranes were formed as previously described (23). The whole-cell configuration was achieved by a sharp suction pulse immediately after seal formation to rupture the plasma membrane within the seal. In this configuration, the soluble cytosolic contents are dialyzed by the pipette filling solution. The pipette solution was 120 mM *N*-methyl-D-Glucamine (NMDG) glutamate, 5 mM Hepes, 1 mM EGTA, 1 μM free Ca^{2+}, pH 7.0, for most experiments. The bath solution was 150 mM NMDG glutamate, 5 mM Hepes, 1 mM EGTA, 1 mM free Ca^{2+}, and the pH was adjusted to 7.0 with either NaOH or HCl. Under these conditions, the principal membrane permeant ion was Ca^{2+}, and the only ionic gradient was the Ca^{2+} because both pipette and bath solutions were made from the same pH adjusted stock solutions. The pipette solution was made hypotonic to prevent cell swelling after formation of the whole-cell configuration (59). Leak currents were determined for each cell using the current measured at the equilibrium potential for Ca^{2+} ($E_{Ca^{2+}}$ = +90 mV), where all of the current could only be leak. The ohmic conductance (linear slope) between $E_{Ca^{2+}}$ (where all of the current was leak), and 0 mV (where, by definition, there can be no leak current) was used to determine the magnitude of the leak current at each test potential, which was subsequently subtracted from all records to yield uncontaminated Ca^{2+} current. Liquid junction potentials between the pipette and bath solutions were balanced immediately before giga-ohm seal formation. Capacitance and series resistance were compensated immediately after formation of the whole-cell configuration, and not altered for the duration of any single experiment, even though perfusion of the bath changed the height of the solution consequently altering the capacitive properties of the whole-cell preparations.

The experimental conditions specified a theoretical membrane potential of +90 mV (i.e., the equilibrium potential for Ca^{2+} which would be achieved in a perfect system, with 0 leak). The actual membrane potential (measured by current clamping the cell to 0 current) was +60 mV, due to a small amount of leak permeability. Therefore, cells were held at +60 mV. Ca^{2+} currents were elicited from test clamps to membrane potentials as negative as −100 mV, in 20 mV increments. No difference in steady state current was observed at 40 ms or at 750 ms after the initiation of the test clamps so all current-voltage relations were determined from the steady state currents (measured 40 ms after clamping to each test voltage) to avoid contamination from uncompensated capacitance (which subsided within 3 ms after the test clamp was initiated).

In some experiments, PMA (1 mg/ml in DMSO; Sigma Immunochemicals) was included in the bath solution at a final concentration of 1 μg/ml and 4 mM ATP was added to the pipette solution. Cells were similarly treated with the PMA analog, 4α-phorbol 12,13-didecanoate (Sigma Immunochemicals), or appropriately diluted DMSO without a detectable effect on Ca^{2+} conductance.

Fura-2 Fluorescence Microscopy

$CD20^+$ and $CD20^-$ cells were incubated in RPMI 1640 medium supplemented with 5 μM fura-2/AM at 37°C for 1 h. Cells were washed twice, resuspended in fresh culture medium, and incubated for an additional h to dialyze away residual acetomethyl ester form of the dye (56). Dye-loaded cells were plated in a perfusion chamber mounted on the stage of an Olympus IMT2 inverted microscope fitted with a quartz light path to facilitate 340 nM UV light. Excitation wavelengths of 340 and 380 nM with 2-nM bandwidths were generated with a dual excitation spectrophotometer (Photon Technologies, Inc., Princeton, NJ). The emission wavelength was 510 nM. Single cells were isolated from the remainder of the field using a variable diaphragm. Photon counts were performed on individual cells using a microscope-adapted Leitz photometer system. The photon counting system and spectrophotometer were under computer control (IBM AT) using software from Photon Technologies, Inc.

Measurements of cytosolic Ca^{2+} were obtained on individual cells. Cell-free areas were measured to determine the background fluorescence. Experiments were only conducted when the cell/background fluorescence ratio exceeded 10:1. Measurements obtained at each wavelength were corrected for background before determination of the 340:380 ratio. Cytosolic Ca^{2+} was calculated as previously described using in vitro determinations of the maximum and minimum ratios (21).

Statistical Analysis

Statistical significance of results was determined using the paired *t* test.

Results

Expression of CD20 by cDNA-transfected Cell Lines

Human cDNA encoding the entire translated region of the CD20 gene was subcloned into a retrovirus vector and transfected into two human T lymphoblastoid cell lines (Jurkat and Rex), a murine pre-B lymphoblastoid cell line (300.19) (1), a human erythroleukemia cell line (K562) (27), and the murine NIH-3T3 fibroblast cell line. In each case, stable oligoclonal cell lines that expressed CD20 were isolated, with the exception of Jurkat, which was clonal (Fig. 1). More than 95% of the cells from each line expressed CD20, as de-

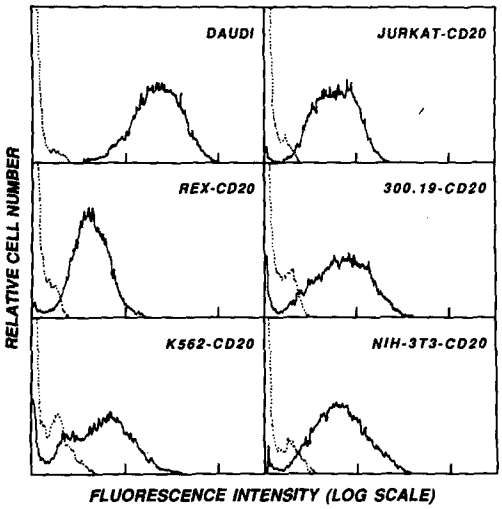

Figure 1. CD20 expression by cell lines transfected with CD20 cDNA. Cells were assessed for expression of CD20 by indirect immunofluorescence staining with the anti-Bla mAb with subsequent flow cytometry analysis. The upper left panel histograms show CD20 expression by Daudi lymphoblasts (——) and an antibody control using unreactive mouse IgG antibody (-----). The other histograms are of paired transfectant cell populations of 10,000 cells each, showing plasma membrane expression of CD20 (——) and lack of CD20 expression in vector-only transfected control cells (-----).

termined by immunofluorescence analysis using a CD20-specific mAb (anti-Bla) (43). Daudi cells endogenously express an average of 60,000 CD20 molecules per cell, and the transfected cells expressed up to ~30,000 CD20 molecules per cell. The highest levels of expression were consistently observed with 3T3-CD20 cells >300.19-CD20 cells = the Jurkat-CD20 clone >K562-CD20, with Rex-CD20 cells expressing the least CD20 of all transfected cell lines generated. The original phenotypes of the parent cell lines were preserved because the transfected cells expressed the same surface markers present in the parent lines. Parental cells were also transfected with the retroviral vector lacking the CD20 cDNA insert to produce parallel cell lines which served as controls for subsequent physiological comparisons (Fig. 1). The establishment of transfected cell lines which expressed CD20, and their respective vector-transfected controls provided matched cells that differed by a single variable (i.e., expression of CD20) and were designated $CD20^+$ and $CD20^-$, respectively.

Phosphorylation of CD20 Expressed by cDNA-transfected Cells

Since CD20 is a dominant phosphoprotein in B cell lines and phosphorylation may be a potential means of CD20 regulation, the ability of CD20 to serve as a substrate for phosphorylation in ectopic cell lines was examined to confirm that the transfected gene product retained the biochemical properties of endogenously expressed CD20. CD20 immunoprecipitated from [^{32}P]orthophosphate-labeled cells demonstrated that CD20 was constitutively phosphorylated in transfected cells just as was found in normal B lymphoblastoid cells (Daudi) (Fig. 2). Treatment of $CD20^+$ transfectants with PMA also induced the same shift in M_r as occurs with CD20 endogenously expressed by B cell lines (Fig. 2), confirming that activation of protein kinase C results in increased phosphorylation of transfected CD20 (53). These findings also demonstrate that the different relative molecular weight species of CD20 result from the differential post-translational processing of a common protein because transfected cells express multiple CD20 species that are identical to those found in B lymphoblastoid cells (47, 53).

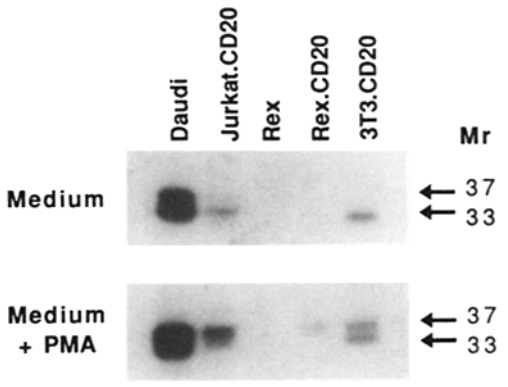

Figure 2. Endogenous phosphorylation of CD20 and changes in phosphorylation following activation of protein kinase C. CD20 was immunoprecipitated from Daudi cells and CD20 cDNA-transfected cell lines cultured with [^{32}P]orthophosphate and analyzed by SDS-PAGE with subsequent autoradiography. CD20 was constitutively phosphorylated to some degree in all cell types and treatment of the cells with PMA shifted the relative proportion of labeled CD20 from the M_r 33,000 form to the 35,000–37,000-M_r forms. Vector-transfected Rex cells do not express CD20 and were included as a negative control.

The extent of CD20 phosphorylation in transfected cells was consistently less than in $CD20^+$ B lymphoblastoid cell lines. One explanation for this finding is that phosphorylation of CD20 in exogenous cell types might be less efficient. Alternatively, the transformations responsible for producing malignant B lymphoblastoid cells may enhance the expression or activity of specific kinases or phosphatases in B cell lines, resulting in hyperphosphorylation of CD20.

$CD20^+$ Jurkat Cells Express Nascent Transmembrane Ca^{2+} Currents

Whole-cell patch-clamp (23) was used to measure plasma membrane ion currents in $CD20^+$ and $CD20^-$ Jurkat transfectants to determine whether expression of CD20 could alter transmembrane Ca^{2+} movement. When Jurkat cells were bathed in culture medium, ionic currents were observed in response to voltage pulses ($^-$100 to $^+$100 mV in 20 mV increments from a holding potential of 0 mV) in $CD20^+$ cells which were absent in $CD20^-$ cells (Fig. 3, *A* and *B*), indicating that the expression of CD20 increased plasma membrane ionic conductance. The inward currents in $CD20^+$ cells were eliminated when the bath Ca^{2+} was chelated to a calculated final concentration of 6 nM with EGTA. Perfusion of the bath solution with Ba^{2+} increased the magnitude of the currents. Subsequent perfusion with EGTA-supplemented culture medium eliminated the currents, thereby confirming that Ba^{2+} was the charge carrier and that Ba^{2+} perfusion specifically altered the plasma membrane conductance. This is not surprising as Ca^{2+} channels typically conduct Ba^{2+} to a greater degree than Ca^{2+} (22). The exponential decays in the transient currents when Ca^{2+} and Ba^{2+} were the charge carriers was examined. The time constant of current decay to steady state was 0.42 ms when Ca^{2+} was the charge carrier and 0.46 ms when Ba^{2+} was the charge carrier. The similarity in the rate of decay of the transient current indicates that the channels through which the current passed were unaffected by the different charge carriers. Therefore, the increased peak transient current in the presence of Ba^{2+} may simply reflect the relative ease with which Ba^{2+} flows through open CD20-associated channels. These findings indicate that the increased current induced by ectopic expression of CD20 was carried specifically by Ca^{2+}. However, contributions from Na^+ or Cl^- to the inward current in $CD20^+$ cells could not be completely excluded because the electrochemical gradients for these ions are appropriately oriented.

To specifically examine transmembrane Ca^{2+} currents in the transfected Jurkat cells, all other permeant ions were eliminated from the bath and pipette solutions by using NMDG glutamate bath solutions. $NMDG^+$ is an organic cation that is impermeant to the membrane, and likewise, $glutamate^-$ is also an impermeant organic anion. Since these ions can not carry current across the plasma membrane, they do not contribute to the membrane potential. Ca^{2+} served as the only ion carrier in the bath solution (1 mM free Ca^{2+}) and the pipette solution was buffered to 1

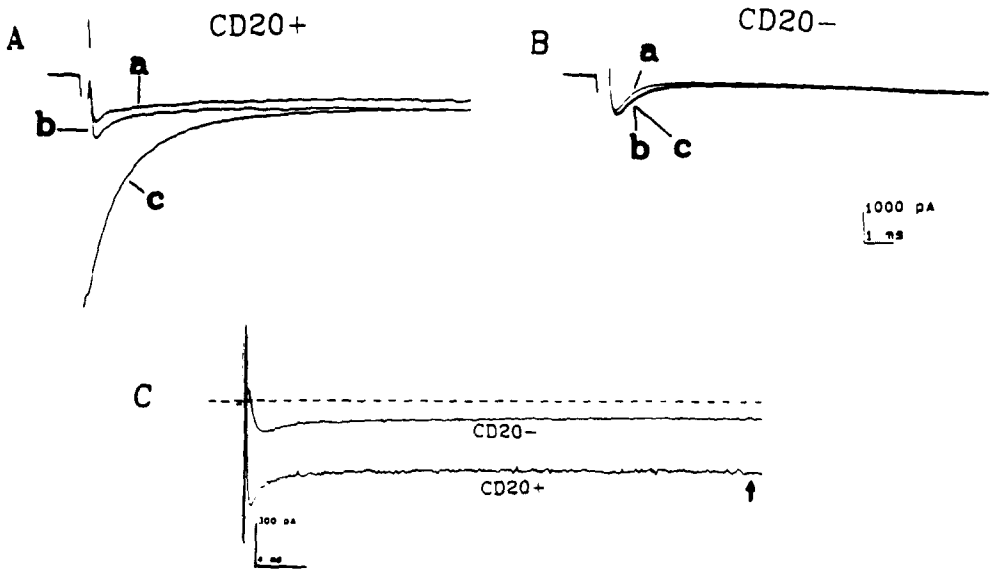

Figure 3. CD20-associated inward whole-cell currents from transfected Jurkat lymphoblasts. The bath solution contained a 1:1 mixture of DME/F12 culture medium (free Ca^{2+} = 0.4 mM), the same medium supplemented with 5 mM EGTA (free Ca^{2+} = 6 nM) or 2 mM Ba^{2+} as indicated. All experiments were performed at 24 ± 2°C. The currents shown in *A* and *B* were elicited to hyperpolarizing voltage clamps to a membrane potential of $^{-}$100 mV from a holding potential of 0 mV. (*A*) Three currents obtained from the same $CD20^{+}$ clone. Current *b* was recorded when the bath contained unsupplemented culture medium. Perfusion with EGTA-supplemented culture eliminated the Ca^{2+} and the current (current *a*). Perfusion with Ba^{2+}-supplemented (2 mM) culture medium increased the current (current *c*). All effects on the current were reversible. (*B*) Typical currents (*a*, *b*, and *c* as described above) from a single CD20-transfected Jurkat clone, showing that the control ($CD20^{-}$) transfectants did not express the current observed in the $CD20^{+}$ transfectants. (*C*) Whole-cell Ca^{2+} currents from $CD20^{+}$- and $CD20^{-}$- transfected Jurkat lymphoblasts generated in response to hyperpolarizations to $^{-}$100 mV from a holding potential of $^{+}$60 mV. The dashed line indicates the 0 current level. Ca^{2+} was the only membrane-permeant ion in the pipette and bath solutions, which contained NMDG-glutamate. The smaller current typifies the currents observed in $CD20^{-}$ cells. The larger current typifies the currents observed in $CD20^{+}$ cells. The arrow indicates the point at which all steady state currents were measured (40 ms after initiation of the test clamp).

μM free Ca^{2+} with EGTA. Therefore, the theoretical equilibrium potential ($E_{Ca^{2+}}$) across the plasma membrane was $^{+}$90 mV. Under current clamp (to 0 current) the actual membrane potential was consistently measured at approximately $^{+}$60 mV, close to the $E_{Ca^{2+}}$, indicating that the predominant conductance was Ca^{2+} with a relatively small leak conductance. Whole-cell voltage clamps (ranging from $^{-}$100 mV to $^{+}$100 mV in 20 mV increments) from a holding potential of $^{+}$60 mV induced whole-cell currents in $CD20^{+}$ transfectants (Fig. 3 *C*) which were qualitatively similar to those elicited when the bath solution was culture medium (Fig. 3 *A*).

$CD20^{+}$-transfected Cells Show Enhanced Ca^{2+} Conductance

Whole-cell patch clamp recording was also used to examine the Ca^{2+} conductance in Daudi B lymphoblasts (which endogenously express CD20) and of four types of cells (of unrelated origin) that were transfected with CD20. Daudi cells had a voltage-insensitive, inwardly rectified steady-state Ca^{2+} conductance of 660 ± 185 pS/20 pF (Fig. 4 *A*). Conductances were calculated as chords conductance from a test potential of −80 mV. Comparisons of ionic conductance between matched pairs of $CD20^{+}$ and $CD20^{-}$ transfectants were used to determine whether expression of CD20 altered Ca^{2+} conductance specifically, and for comparison with the Ca^{2+} conductance of cells which endogenously express CD20. The qualitative and quantitative findings of whole-cell patch clamps on CD20-transfected cells and their respective controls indicate that in four of the cell types (Jurkat, 300.19, K562, and NIH-3T3) expression of CD20 increased plasma membrane Ca^{2+} conductance (Fig. 4, *B–F*). Further, the Ca^{2+} conductances of $CD20^{+}$ cells were qualitatively similar to the Ca^{2+} conductance of Daudi B lymphoblasts. The current–voltage relations indicated that the Ca^{2+} conductance was not voltage dependent, but the currents were inwardly rectified at hyperpolarizing membrane potentials ($^{-}$80 mV and $^{-}$100 mV). These findings indicate that expression of CD20 endows a variety of cells of different lineages with the same Ca^{2+} conductance that is present in cells which endogenously express CD20. The fifth transfected cell type (Rex) showed no significant increase in Ca^{2+} conductance between $CD20^{+}$ cells and $CD20^{-}$ cells (Fig. 4C). However, Rex-CD20 cells expressed approximately five times less CD20 than the other transfected cell lines (Fig. 1). The mean Ca^{2+} conductance in each of the cell types correlated well with the average amount of CD20 expressed by each cell type (r = 0.814) suggesting that Rex-CD20 cells did not express enough CD20 to increase the plasma membrane Ca^{2+} conductance to detectable levels. Therefore, the most likely explanation for the increased Ca^{2+} conductance associated with CD20 expression is that CD20 itself is a Ca^{2+} channel.

CD20 Expression Alters Cytosolic-free Ca^{2+} Activity

Since membrane expression of CD20 correlated with an increase in transmembrane Ca^{2+} conductance, changes in intracellular free Ca^{2+} concentration were also examined. $CD20^{+}$ and $CD20^{-}$ Jurkat transfectants were loaded with the Ca^{2+}-sensitive fluorophore, fura-2. The cells were ex-

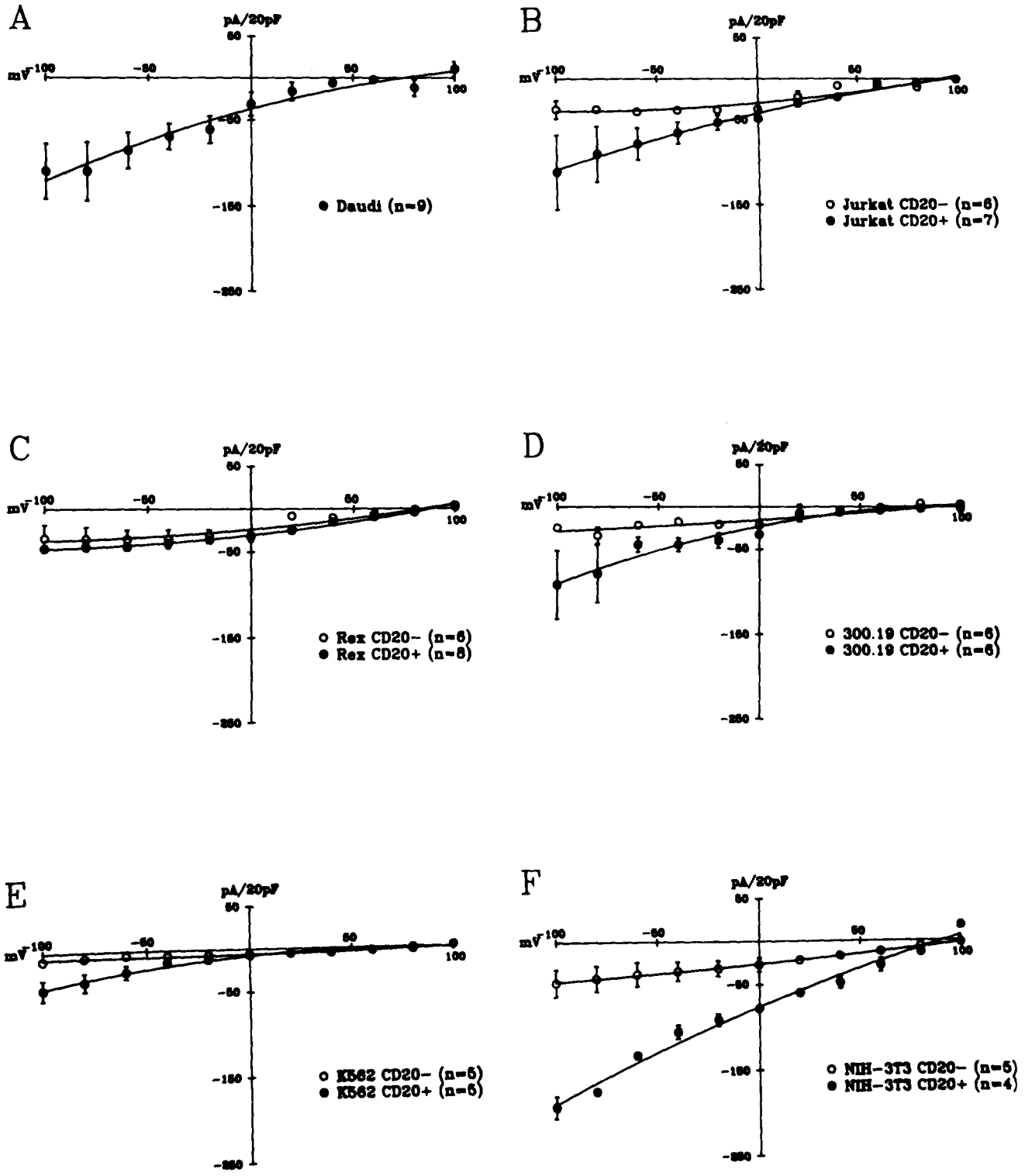

Figure 4. Leak-subtracted steady-state current-voltage relations for cells expressing CD20. (*A*) Daudi lymphoblasts, which constitutively express CD20, typically had an inward rectified voltage-insensitive Ca^{2+} conductance. (*B*) $CD20^+$ and $CD20^-$ transfected Jurkat cells. The expression of CD20 added a voltage-insensitive, inward rectified component to the whole-cell Ca^{2+} current. (*C*) Typically Rex cells had little Ca^{2+} conductance (75% of the cells), and the expression of CD20 did not significantly increase the conductance. However, Rex cells expressed very little CD20 compared to Daudi cells or any of the four other transfected cell lines. Therefore the lack of a significant CD20-associated current in Rex cells was most likely due to the low levels of CD20 expression. (*D*) $CD20^+$ and $CD20^-$ mouse 300.19 pre-B cells. The effect of CD20 on the Ca^{2+} current in these cells was identical to the effect observed in transfected Jurkat cells. (*E*) The current-voltage relations from $CD20^-$ and $CD20^+$ K562 erythroleukemia cells show the typical increase in inward rectified voltage-insensitive Ca^{2+} conductance associated with the expression of CD20. (*F*) Expression of CD20 by NIH-3T3 fibroblasts induced a greater than fourfold increase in Ca^{2+} conductance (238 $\pm$ 95 pS, $n = 5$ for $CD20^-$ cells; 955 $\pm$ 39, $n = 4$ for $CD20^+$ cells) which was qualitatively similar to the non-voltage-dependent inward rectified Ca^{2+} conductance associated with CD20 in Daudi cells and each of the transfected cell lines.

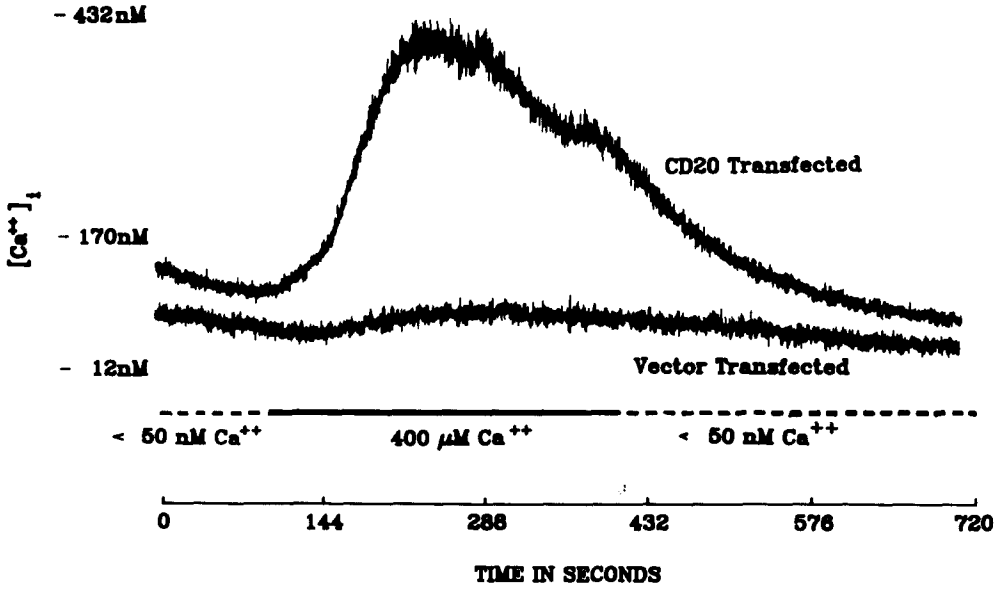

Figure 5. Fura-2 fluorescence measurements of cytosolic-free Ca^{2+} activity in $CD20^+$- and $CD20^-$-transfected Jurkat lymphoblasts. The horizontal bar indicates the perfusion protocol and the results shown are from representative single cells. Increasing the extracellular Ca^{2+} concentration from 50 nM to 400 μM induced a large intracellular free Ca^{2+} activity increase in $CD20^+$ cells and only a small increase in $CD20^-$ cells, directly demonstrating that expression of CD20 increased plasma membrane Ca^{2+} permeability. These results are representative of those obtained in four separate experiments.

amined by dual-excitation, single-emission fluorescence microscopy and compared to determine whether the expression of CD20 altered the steady-state cytosolic Ca^{2+} activity. $CD20^+$ cells had a significantly higher cytosolic Ca^{2+} activity than $CD20^-$ cells (124 ± 47 nM, n = 20 in $CD20^+$ cells, vs. 58 ± 45 nM, n = 20, in $CD20^-$ cells: $P < 0.001$). Fura-2–loaded cells were preincubated in Ca^{2+}-depleted culture medium (5 mM EGTA added) and then re-exposed to extracellular Ca^{2+} (400 μM) by perfusion with normal culture medium. $CD20^+$ transfectants had a sixfold greater rate of increase in intracellular free Ca^{2+} activity in response to re-exposure to Ca^{2+}, compared to the $CD20^-$ controls (Fig. 5). This observation is consistent with the hypothesis that CD20 expression increases plasma membrane Ca^{2+} permeability, which accordingly accounts for the increased steady state cytosolic Ca^{2+} activity.

mAb Binding to CD20 Increases Ca^{2+} Conductance

The binding of the anti-Bla mAb to CD20 on B lymphocytes alters cell cycle progression of mitogen-activated B lymphocytes suggesting that it dysregulates a required process (51). However, treatment of B lymphoblastoid cell lines with the anti-Bla mAb does not affect the growth of transformed cells. Therefore, Daudi B lymphoblastoid cells were used to determine whether mAb binding to CD20 could affect Ca^{2+} conductance. The Ca^{2+} current in Daudi cells was not acutely altered by their exposure to saturating concentrations of the CD20-specific anti-Bla mAb (25 μg/ml for up to 15 min). However, in a paired comparison, Daudi cells incubated with anti-Bla mAb (25 μg/ml) for 24 h had a steady-state inward conductance of 976 ± 341 pS/20 PF (n = 3) at hyperpolarizing clamp steps, compared to 424 ± 82 pS/20 pF (n = 6) in cells not exposed to the CD20 mAb ($P < 0.05$). This effect appeared specific for CD20 because similar changes were not observed in cells treated with an isotype-matched mAb, HB-5, that binds to cell-surface CD21 on B cells. These results indicate that binding of the anti-Bla mAb to CD20 did not cause acute alterations in Ca^{2+} currents. However, the findings clearly demonstrate that chronic treatment alters Ca^{2+} homeostasis which could account for the mAb-induced effects on B lymphoblast cell growth/cell cycle.

Previous studies failed to detect significant changes in intracellular free Ca^{2+} activity immediately after anti-Bla mAb binding to CD20 on spleen B lymphocytes (51). However, the effects of long-term exposure to the mAb on cytosolic Ca^{2+} have not been previously examined. Therefore, the effects on cytosolic Ca^{2+} activity resulting from anti-Bla mAb binding to CD20 for 24 h were examined in fura-2–loaded Daudi cells. As previously described, culturing cells with the anti-B1 (CD20) mAb resulted in redistribution of the surface antigen into patches, but did not down-modulate surface expression or appear to result in receptor internalization (31, 51). Cells cultured without anti-Bla mAb present had an average steady-state cytosolic Ca^{2+} activity of 46 ± 15 nM (n = 30). Incubation of the cells for 24 h with saturating amounts of the anti-Bla mAb (25 μg/ml) significantly increased the cytosolic Ca^{2+} activity to 123 ± 80 nM (n = 30; $P < 0.001$). These results are consistent with the electrophysiological observations that 24 h was required for anti-B1 mAb binding to increase plasma membrane Ca^{2+} conductance.

In contrast to the anti-Bla mAb, binding of the 1F5 mAb, which recognizes a CD20 epitope that is different from the epitope bound by the anti-Bla mAb (48), causes acute changes in activation/signal transduction of normal B cells (10, 40). Consistent with this, exposure of Daudi cells to the 1F5 mAb (25 μg/ml), acutely increased Daudi cell whole-cell Ca^{2+} current (within 1 min) (Fig. 6). Thus, mAb binding of 1F5 to the CD20 molecule appears to directly alter Ca^{2+} current. These direct electrophysiological observations confirm that mAb binding to different epitopes on CD20 can induce either acute or delayed changes in Ca^{2+} current. It was also observed that 1F5 mAb treatment had no net acute effect on the cytosolic Ca^{2+} activity in Fura-2–loaded Daudi cells consistent with earlier publications (20). Therefore, because of Ca^{2+} buffering activity within

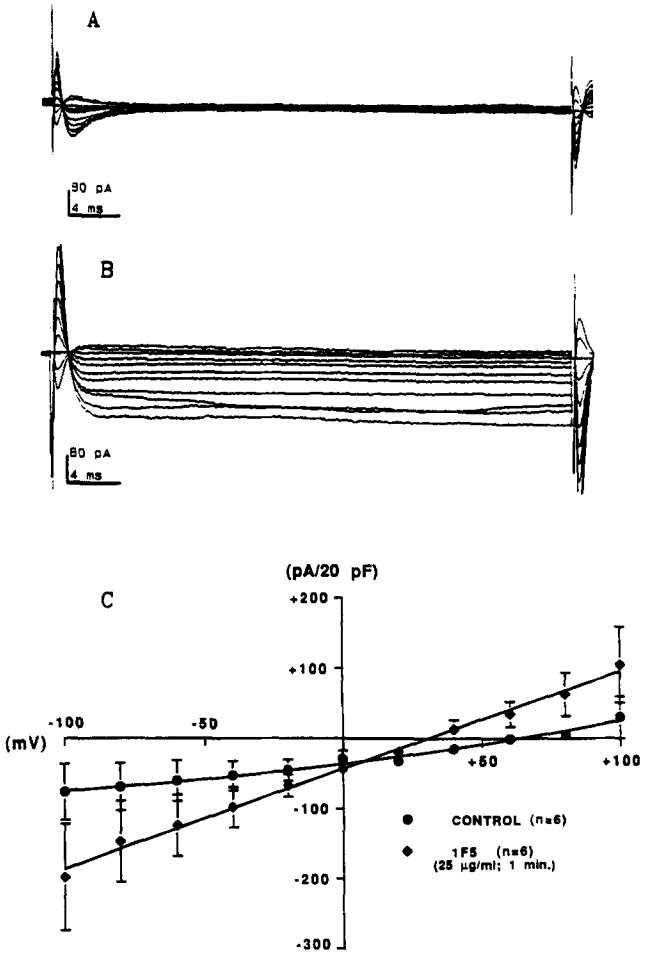

Figure 6. The effect of 1F5 mAb binding to CD20 on whole-cell Ca^{2+} current in Daudi lymphoblasts. (*A*) Whole-cell Ca^{2+} currents generated in response to test voltages of $^{-}100$ mV to $^{+}100$ mV in 20 mV increments from a holding potential of $^{+}60$ mV. (*B*) Whole-cell Ca^{2+} currents from the same cell described in *A*, 1 min after exposure to CD20-specific mAb (1F5; 25 μg/ml). Capacitance was compensated immediately after the whole-cell configuration was formed and was not recompensated during the course of the various perfusions, because this compensation could artifactually alter whole-cell currents. (*C*) Steady state current-voltage relations before and after 1F5 mAb exposure measured at 45 ms. Values represent the average current-voltage relations (±SEM) obtained in six experiments.

cytoplasm, the voltage clamp finding may not directly reflect the total effect of 1F5 on in vivo Ca^{2+} homeostasis.

Binding of mAb to CD20 Alters Cell Cycle-dependent Changes in Cytosolic Ca^{2+} Activity

Binding of the anti-Bla mAb to normal B lymphocytes blocks the transition of cells from the G1 phase of cell cycle into the S-G2/M phases, but does not alter cell-cycle progression in transformed B lymphoblastoid cells (51). Similarly, changes in intracellular free Ca^{2+} activity also accompany cell cycle progression with G_1 phase B lymphoblastoid cells having higher levels of intracellular free Ca^{2+} activity that returns to lower levels with cell cycle progression (Bubien, J. K., and P. D. Bell, manuscript in preparation). Therefore, to determine whether mAb binding to CD20 alters the normal changes in cytosolic Ca^{2+} activity that occur with cell cycle progression, Daudi cells were suspended at the G1-S stage of cell cycle by treatment with hydroxyurea (1 mM for 24 h). The mean free cytosolic Ca^{2+} activity was 42 ± 14 nM (n = 10) in these cells, whereas the cytosolic Ca^{2+} activity of cells from the same population 24 h after release from hydroxyurea block was significantly lower (27 ± 3 nM, n = 10; P = 0.002). In paired trials, the cytosolic Ca^{2+} activity of G1-S phase cells also cultured with the anti-Bla mAb was the same as the control hydroxyurea-treated cells. However, the mean cytosolic Ca^{2+} activity of cells that were released from hydroxyurea for 24 h in the presence of the anti-Bla mAb was 55 ± 25 nM (n = 10). These results directly demonstrate that binding of the anti-Bla mAb to CD20 prevented a decrease in cytosolic free Ca^{2+} activity as the cells progressed beyond G_1-S of the cell cycle, as was observed in the control cells. Thus, one potential mechanism whereby mAb binding to CD20 may disrupt normal cell-cycle progression could be by altering CD20-associated cell cycle–dependent Ca^{2+} homeostasis.

PMA Treatment Reduces CD20 Associated Ca^{2+} Conductance

Daudi cells were whole-cell clamped as previously described with NMDG-glutamate bath and pipette solutions. The Ca^{2+} concentration of the bath solution was 1 mM and 1 μM in the pipette solution with all voltage clamp and leak subtraction protocols used as previously described. After assessing the control CD20-associated Ca^{2+} conductance, the cells were perfused with a bath solution supplemented with 1 μM PMA and the whole-cell CD20–associated Ca^{2+} conductance was assessed by voltage clamp at 1 min (Fig. 7). PMA treatment reduced the whole-cell CD20–associated Ca^{2+} conductance from 520 ± 125 pS/20 pF to 406 ± 111 pS/20 pF after 1 min. A reduction in the conductance was observed in eight out of nine cells, and one cell had a very

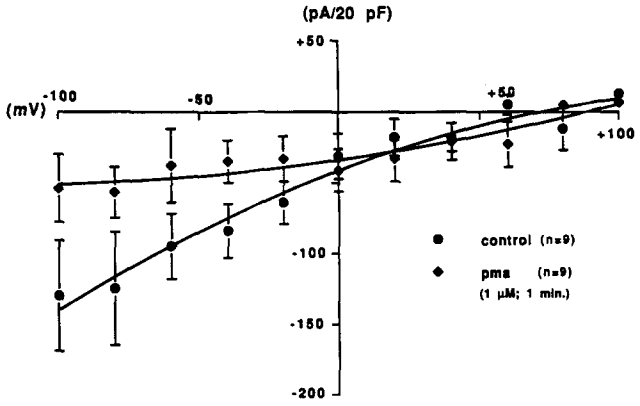

Figure 7. The effect of PMA treatment on CD20-associated Ca^{2+} current in Daudi cells. Values represent the mean current-voltage relations (±SEM) obtained in paired experiments in eight out of nine cells tested. Control values represent untreated cells, while PMA (1 μM) treatment decreased the currents 1 min after exposure. In control experiments where cells were treated with a 4α-phorbol ester analogue (1 μM) or carrier solution (diluted DMSO) the current-voltage relations of paired cells were unaffected.

large control conductance (1,461 pS/20 pF) which was reduced to 330 pS/20 pF after PMA treatment. The difference in conductance (113 ± 37 ps/20 pF, $n = 7$) was significant ($P = 0.023$) after these two outlying cells were eliminated from the pool. Although PMA was used at 1 μM because of the acute nature of the experiments and that a functional concentration of PMA had to cross the plasma membrane in a relatively short time, no difference in conductance was observed in control experiments using the 4-α phorbol analogue, that does not activate protein kinase C (data not shown). This finding implies that protein kinase C–mediated phosphorylation of CD20 inactivates CD20-associated Ca^{2+} current, and this may be one molecular mechanism for regulation of transmembrane Ca^{2+} conductance in B lymphocytes.

In Situ Oligomeric Structure of CD20

Immunoprecipitation studies have previously demonstrated that CD20 associates with other cell surface and cytosolic proteins (47, 53). The possibility that CD20 residues in the plasma membrane as a multimolecular complex was investigated by biochemically crosslinking plasma membrane proteins followed by specific immunoprecipitation of CD20 and spatially close (i.e., cross-linked) proteins. Radiolabeled membrane proteins of the B lymphoblastoid cell line, BJAB, were covalently cross-linked with DSP, on ice, to maintain the association of all proteins with exposed proximal primary amino groups within up to 12 A of each other. The cells were then washed and lysed with detergent in the presence of 1% (wt/vol) BSA. Immunoprecipitation of CD20 from the cross-linked membrane proteins revealed three distinct bands 33,000–35,000, 70,000, and 140,000 M_r (Fig. 8 *A*, *arrowheads*). A cell-surface protein of ~31,000 M_r that specifically coprecipitates with CD20 was also observed below the 33,000 M_r CD20 band as previously described (35, 53). The disulfide bond of DSP was subsequently reduced to dissociate the cross-linked proteins and the PAGE gel was again run in a second dimension. After dissociation and electrophoresis, the 70,000 and 140,000 M_r bands migrated to form bands at 33,000–35,000 M_r (Fig. 8 *B*), suggesting that the larger bands represented homodimeric and homotetrameric oligomers of CD20. The band at 31,000 M_r that coprecipitates with CD20 was also visualized. All reactions were carried out in the presence of excess unlabeled protein to insure that the multimeric forms of CD20 were obtained exclusively from the crosslinked membrane proteins. In similar experiments carried out with [^{32}P]orthophosphate-labeled cross-linked cells, each of the bands comprising the monomeric and multimeric forms of CD20 were phosphorylated (data not shown). Immunoprecipitation of MHC class I antigens from the same lysate of cross-linked cells revealed that class I molecules were not cross-linked, thereby indicating that cross-linking of CD20 was specific and that not all cell surface molecules were chemically coupled.

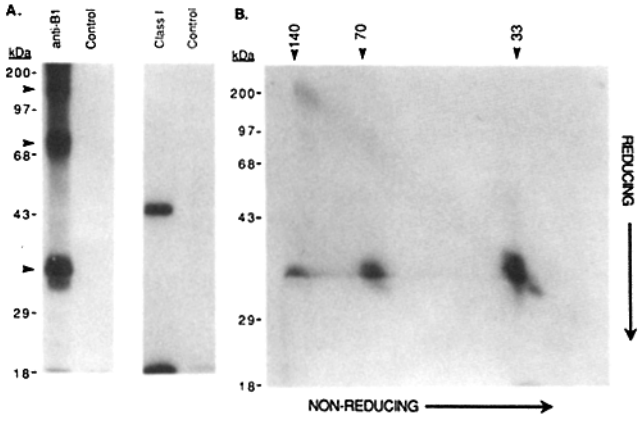

Figure 8. In situ chemical cross-linking of cell-surface molecules with subsequent immunoprecipitation of CD20. (*A*) Three dominant protein bands (33,000, 70,000, and 140,000 M_r, indicated by *arrowheads*) were immunoprecipitated from surface-iodinated B lymphoblastoid cells (BJAB) with the anti-Bla mAb after DSP cross-linking of plasma membrane proteins. Gel analysis of the immunoprecipitated materials was run under non-reducing conditions. The control lanes represent materials precipitated by an isotype-matched unreactive mAb. MHC class I antigens were also immunoprecipitated from the same cell lysate revealing only a single monomeric molecular species. (*B*) Two-dimensional analysis of the materials isolated in *A*. Proteins electrophoresed in the first dimension were treated with reducing conditions (to break the disulfide bond of the cross-linking agent) and run in the second dimension under reducing conditions. Each of the bands identified under non-reducing conditions migrated at 33,000 M_r, indicating that the larger bands were comprised of CD20 monomeric subunits. The relative molecular weight of proteins with known molecular weights are indicated (*kD*).

Discussion

In this report, four complimentary experimental results are presented, each of which indicate that CD20 plays a direct role in regulating plasma membrane Ca^{2+} permeability. First, CD20 cDNA-transfected Jurkat T lymphoblasts, murine 300.19 pre-B lymphoblasts, K562 human erythroleukemia cells, and NIH-3T3 murine fibroblasts all acquired a qualitatively similar Ca^{2+} conductance not present in their respective $CD20^-$ controls (Fig. 3 and 4). The CD20-associated Ca^{2+} currents observed in the transfected cells were identical to Ca^{2+} currents observed in Daudi lymphoblasts which endogenously express CD20. They were also similar to Ca^{2+} currents observed in MHY206 cells (4) and S194 cells (16), both of which are murine B lineage cells, and therefore, presumably endogenously express CD20 (52). Second, the rate of Ca^{2+} influx into Ca^{2+}-depleted Jurkat cells in response to Ca^{2+} reperfusion was six times higher in $CD20^+$ transfectants than matched controls (Fig. 5). Third, expression of CD20 increased the steady-state cytosolic Ca^{2+} activity in transfected Jurkat cells, an expected consequence of enhanced plasma membrane Ca^{2+} permeability. Finally, mAb binding to CD20 increased whole-cell Ca^{2+} currents in B lymphoblastoid cells (Fig. 6). Taken together, these results provide evidence that CD20 is itself a Ca^{2+} channel or directly regulates Ca^{2+} channel activity.

Chemical cross-linking of plasma membrane proteins followed by immunoprecipitation of CD20 revealed that CD20 formed oligomeric complexes in the plasma membrane composed of two and four homologous subunits (Fig. 8). Thereby, CD20 structure and oligomeric complex formation are

similar to what has been previously found for other well-characterized ion channels. The rat brain Na^+ channel subcomponents possess four membrane-spanning domains and the channel complex is composed of four repeating homologous subunits (45). Similarly, the $GABA_A$ receptor Cl^- channel is composed of five repeating homologous subunits, and each subunit has four membrane-spanning domains (36). These properties are also found with the family of glutamate receptor ion channels, which characteristically have four membrane spanning domains and form homomeric and heteromeric channels (41). The acetylcholine receptor subunits also have four membrane spanning domains, but four different subunits assemble into a heteromeric complex of five subunits forming an uncharged channel (12). Thus, the finding that CD20 forms homo-oligomers in the plasma membrane suggests that a multimeric form of CD20 may constitute the functional configuration of the protein.

Three possible models of how CD20 regulates transmembrane Ca^{2+} current are possible. First, CD20 may not itself be a component of a Ca^{2+} channel, but mAb or ligand binding to the CD20 complex may initiate second messenger pathways that regulate transmembrane Ca^{2+} current through endogenous channels. However, in the whole-cell clamp configuration the cytoplasmic contents are dialyzed out of the cell suggesting that cytosolic second messengers such as ATP, cAMP, NO, cGMP, and Ca^{2+} would be removed. While other components such as diacylglycerol, protein kinase C, and protein kinase A would remain within the membrane, signal generation may be inefficient at best. Second, CD20 may be in intimate physical association with a Ca^{2+} channel forming complex and thereby transmit signals directly to the complex to regulate Ca^{2+} flux. The third possibility is that the CD20 complex itself is the ion channel. The third possibility is best supported by the data as endogenous Ca^{2+} channel activity similar to that found in B lymphoblastoid cells was not found in T lymphoblasts, erythroleukemia cells or fibroblasts, arguing against the presence of a similar channel endogenous to these disparate cell types that was only detected when CD20 was present. Furthermore, since the expression of CD20 in heterologous cell types generated a qualitatively similar channel activity to that found endogenously in B lymphocytes, it is likely that it at least forms an essential component of a channel complex expressed by B lymphocytes. Furthermore, the strategy of ectopic expression of cDNA resulting in the generation of nascent channel activity or reconstitution of channel activity has been used repeatedly to verify the isolation of cDNA encoding ion channels or their subunits (29, 30, 34, 36, 46).

These experiments do not unambiguously prove whether or not CD20 itself is a Ca^{2+} channel. Unfortunately, at the present time there is no single experiment or set of experiments which can answer this question. While isolation of pure CD20 and incorporation of CD20 into planar lipid bilayers could be a means of directly addressing this question, this requires the biochemical purification of CD20 to homogeneity. A purification protocol without use of CD20-specific mAb has not yet been successfully developed as conditions which remove the CD20 protein from the CD20 mAb appear to denature CD20 structure. In addition, polypeptides not thought to have membrane-spanning regions such as the first nucleotide binding domain of cystic fibrosis transmembrane regulator protein can form ion-conductive pores in planar lipid bilayers (2), casting doubt on the perception that reconstitution of a protein into planar lipid bilayers and the subsequent measurement of an ionic conductance is definitive. Further, such experiments provide no assurance that the tertiary or quaternary structure of the isolated protein is preserved during the isolation procedure or that necessary cellular components that regulate channel function are co-purified. Given all of these constraints, it is possible that such experiments may be less definitive than the paired transfectant experiments presented in this study where CD20 was expressed by ectopic cell types and a similar nascent channel activity was detected in all cells expressing high levels of CD20.

Since CD20 itself appears to directly mediate plasma membrane Ca^{2+} conductance in B lymphocytes, it follows that regulation of CD20 can provide a means by which B lymphocytes are able to control plasma membrane Ca^{2+} influx. Phosphorylation may be one molecular mechanism used by B lineage cells to regulate CD20 function. CD20 expressed by transfected cells was constitutively phosphorylated to some extent and PMA-induced activation of protein kinase C increased the extent of phosphorylation thereby increasing the apparent molecular weight of the ectopic protein (Fig. 2) as occurs with endogenously expressed CD20 (47). Many ion channel proteins are phosphorylated, and their functions are presumably affected by the degree to which they are phosphorylated and the site of phosphorylation. The Na^+ channel, the acetylcholine nicotinic receptor K^+ channel, and the dihydropyridine-sensitive Ca^{2+} channel proteins are all phosphorylated by both cyclic AMP-dependent protein kinase and protein kinase C (30). Phosphorylation directly alters the open probability of the dihydropyridine-sensitive Ca^{2+} channel (14). Similarly, the function of CD20 may be directly modified by phosphorylation. In the present study, PMA treatment significantly reduced CD20-associated Ca^{2+} conductance (Fig. 7). However, it is possible that phosphorylation of CD20 on other residues by other kinases may have positive effects on CD20 function. Alternatively, phosphorylation of CD20 may be only one component of a more complex regulatory mechanism such as oligomer association or dissociation. For example, an oligomeric channel complex may be formed from a pool of monomeric CD20 as the monomers become phosphorylated or dephosphorylated. Phosphorylation-mediated regulation of CD20 function could also be a dynamic process involving multiple kinases that are differentially activated during cell cycle progression.

Whole-cell Ca^{2+} currents remarkably similar to CD20-associated currents have been observed in mast cells and termed I_{CRAC} (calcium release-activated calcium) (24). The Ca^{2+} currents observed in mast cells are inwardly rectified, tend to partially inactivate with time, and are about 50–100 pA when the cells are hyperpolarized to −100 mV. CD20-associated Ca^{2+} currents had identical characteristics. One apparent difference between the I_{CRAC} currents and CD20-associated currents is the ability of Ba^{2+} to carry the current. In the case of CD20-associated current, Ba^{2+} appears to carry the current at least as well as Ca^{2+} (Fig. 3), while in mast cells, Ba^{2+} appears to inhibit the I_{CRAC} current. The striking similarity between the CD20-associated Ca^{2+} currents in B lymphocytes and the I_{CRAC} Ca^{2+} currents observed in mast cells suggests that similar proteins may account for

these currents. Since mast cells express the $F_{\epsilon}RI$ β chain, which has amino acid sequence homology and a similar hydropathy profile to CD20, it is possible that CD20 and the $F_{\epsilon}RI$ β chain could have similar functional properties.

CD20 expressed by B lineage cells associates with other plasma membrane proteins, providing a possible mechanism for the normal regulation of CD20 function. Immunoprecipitation studies show that CD20 associates with a cell-surface protein of 29,000–31,000 M_r (Fig. 8), four cytoplasmic proteins in the relative molecular weight range of 50,000–60,000 and variably with a large cell surface protein (180,000–200,000 M_r) in B lymphoblasts (35, 53). However, transfection of CD20 alone appears to be sufficient for the induction of Ca^{2+} conductance in non-B lineage cells, because none of these proteins were detected in immunoprecipitations of CD20 in transfected T lymphoblasts (data not shown). This would suggest that coexpression of these proteins is not required to reconstitute the CD20-associated Ca^{2+} conductance. However, these findings do not rule out the possibility that accessory proteins play a role in regulating CD20 function and that other endogenous regulatory molecules present in all cell types can affect CD20 activity. Accessory proteins present in the channel complex are important for the regulation of rat brain Na^+ channels (34) and the dyhydropyridine-sensitive Ca^{2+} channel (46). These channels are composed of homologous and heterologous subunits. However, only single subunit types are required to reconstitute channel function in ectopic expression systems. The other subunits appear to only be necessary for regulation of channel function (29). This may explain why the CD20-associated Ca^{2+} conductance was always found in an active configuration. Since, CD20 is related to the $F_{\epsilon}RI$ β chain, it is possible that, as with the $F_{\epsilon}RI$ complex, additional ligand-binding components that associate with CD20 will be identified.

Cytosolic Ca^{2+} and cation channel activity vary with the cell cycle in lymphocytes, with cytosolic Ca^{2+} being low in G_0 and S and increased threefold in G_1 (5, 6). Therefore, the finding that CD20 mediates or regulates a transmembrane Ca^{2+} conductance could provide a mechanistic explanation for the different biological effects of two CD20 mAb, 1F5 and anti-Bla, which are both monospecific for CD20. Binding of the 1F5 mAb to CD20 activates resting tonsillar B lymphocytes (10); while binding of the anti-Bla mAb has no effect on resting cells (50). The binding of each mAb to CD20 blocks cell cycle progression of mitogen-activated blood B cells (50). The voltage-clamp studies shown in this study indicate that binding of either mAb to CD20 increased B lymphoblast Ca^{2+} current. 1F5 mAb binding to CD20 acutely increased Ca^{2+} conductance (within 2 min). The ability of 1F5 mAb to activate dense tonsillar B lymphocytes (10) is consistent with the finding that Ca^{2+} influx is required for B lymphocyte activation (28). The 1F5 mAb-induced increase in Ca^{2+} conductance may therefore activate resting B lymphocytes by facilitating Ca^{2+} entry, similar to Ca^{2+} ionophore-induced activation (28). In contrast, binding of the anti-Bla mAb failed to alter the basal Ca^{2+} conductance, and coincidentally does not activate resting B lymphocytes (50). However, prolonged incubation of B cells with anti-Bla mAb did increase both Ca^{2+} conductance and steady state cytosolic Ca^{2+} activity. These findings are consistent with the notion that B lineage cells differentially regulate CD20 activity as a function of cell cycle progression. Also, steady state cytosolic Ca^{2+} activity decreased as synchronized B lymphoblasts progressed beyond G_1-S of the cell cycle in the absence of anti-Bla mAb. However, after incubation with anti-Bla, the CD20-associated Ca^{2+} current increased and the cytosolic Ca^{2+} activity remained elevated. The different biological effects of the anti-Bla and 1F5 mAb imply that mAb-induced alterations of the endogenous regulation of CD20 affect plasma membrane Ca^{2+} conductance as well as cytosolic Ca^{2+} homeostasis in B lineage cells.

Many channels are regulated by conformational changes that result in opened or closed channels, suggesting that the binding of the anti-CD20 mAb may affect the conformation of the CD20 subunits. The binding of 1F5 mAb to CD20 may mimic the effect of a modulatory ligand to induce structural changes in CD20 which in turn results in the formation of a conductive configuration of the protein/complex. In contrast, anti-Bla mAb binding appears to stabilize the CD20-mediated Ca^{2+} conductance, but the mAb does not have the ability to acutely enhance the conductance. Similar findings have been described with the acetylcholine receptor/channel where molecules that mimic acetylcholine (agonists) stabilize the channel in the open position while those that antagonize acetylcholine stabilize the channel in a closed position (9). The direct effects of anti-Bla and 1F5 mAb on CD20-associated Ca^{2+} currents are consistent with the hypothesis that CD20 functions as a Ca^{2+} channel. Although future studies will focus on the purification of the CD20 protein and its reconstitution into artificial cell membranes, expression of the CD20 protein in ectopic cell types as described in this study directly implicates CD20 in the regulation of transmembrane Ca^{2+} conductance in B lymphocytes.

The authors thank Drs. L. M. Nadler and E. A. Clark for providing mAb, and E. C. Walthall for technical assistance.

This work was supported by National Institutes of Health grants AI-26872 and CA-34183 to T. F. Tedder, DK-31091 to R. A. Frizzell, AM-32032 to P. D. Bell, and a grant from the Cystic Fibrosis Foundation to J. K. Bubien. T. F. Tedder is a Scholar of the Leukemia Society of America.

Received for publication 16 December 1992 and in revised form 17 March 1993.

References

1. Alt, F., N. Rosenberg, S. Lewis, E. Thomas, and D. Baltimore. 1981. Organization and reorganization of immunoglobulin genes in A-MuLV-transformed cells: rearrangement of heavy but not light chain genes. *Cell.* 27:381–388.
2. Arispe, N., E. Rojas, J. Hartman, E. J. Sorscher, and H. G Pollard. 1992. Intrinsic anion channel activity of the recombinant first nucleotide binding fold domain of the cystic fibrosis transmembrane regulator protein. *Proc. Natl. Acad. Sci. USA.* 89:1539–1543.
3. Barnstable, C. J., W. F. Bodmer, G. Brown, G. Galfre, C. Milstein, A. F. Williams, and A. Ziegler. 1978. Production of monoclonal antibodies to group A erythrocytes, HLA and other human cell surface antigens. New tools for genetic analysis. *Cell.* 14:9–20.
4. Bosma, M., and N. Sidell. 1988. Retinoic acid inhibits Ca^{++} currents and cell proliferation in a B-lymphocyte cell line. *J. Cell Physiol.* 135: 317–323.
5. Brent, L. H., J. L. Butler, W. T. Woods, and J. K. Bubien. 1990. Transmembrane ion conductance in human B lymphocyte activation. *J. Immunol.* 145:2381–2389.
6. Bubien, J. K., K. L. Kirk, T. A. Rado, and R. A. Frizzell. 1990. Cell cycle dependence of chloride permeability in normal and cystic fibrosis lymphocytes. *Science (Wash. DC).* 248:1416–1419.
7. Calvo, J., J. Radicella, and E. Charreau. 1983. Measurement of specific radioactivities in labeled hormones by self-displacement analysis. *Biochem. J.* 212:259–264.
8. Cepko, C., B. Roberts, and R. Mulligan. 1984. Construction and applications of a highly transmissible murine retrovirus shuttle vector. *Cell.* 37:1053–1062.

9. Changeuz, J.-P., A. Devillers-Thiery, and P. Chemouilli. 1985. Acetylcholine receptor: An allosteric protein. *In* Neuroscience. Abelson, P., editor. American Association for the Advancement of Science, Washington, D.C. 216–238.
10. Clark, E. A., G. Shu, and J. A. Ledbetter. 1985. Role of the Bp35 cell surface polypeptide in human B-cell activation. *Proc. Natl. Acad. Sci. USA.* 82:1766–1770.
11. Corcia, A., I. Pecht, S. Hemmerich, S. Ran, and B. Rivnay. 1988. Calcium specificity of the antigen-induced channels in rat basophilic leukemia cells. *Biochemistry.* 27:7499–7506.
12. Dani, J. 1989. Site-directed mutagenesis and single-channel currents define the ionic channel of the nicotinic acetylcholine receptor. *Trends Neurosci.* 12:125–128.
13. Einfeld, D. A., J. P. Brown, M. A. Valentine, E. A. Clark, and J. A. Ledbetter. 1988. Molecular cloning of the human B-cell CD20 receptor predicts a hydrophobic protein with multiple transmembrane domains. *EMBO (Eur. Mol. Biol. Organ.). J.* 7:711–717.
14. Flockerzi, V., H.-J. Oeken, F. Hofmann, D. Pelzer, A. Cavalie, and W. Trautwein. 1986. Purified dihydropyridine-binding site from skeletal muscle t-tubules is a functional calcium channel. *Nature (Lond.).* 323:66–68.
15. Forsgren, A., A. Penta, S. F. Schlossman, and T. F. Tedder. 1987. Regulation of B cell function through the CD20 (B1) molecule. *In* Leukocyte Typing III: White cell differentiation antigens. McMichael, A. J., editor. Oxford University Press, Oxford, U. K. 396–399.
16. Fukushima, Y., and S. Hagiwara. 1983. Voltage-gated Ca^{++} channels in mouse myeloma cells. Proc. Natl. Acad. Sci. USA. 80:2240–2242.
17. Genot, E., M. A. Valentine, L. Degos, F. Sigaux, and J. P. Kolb. 1991. Hyperphosphorylation of CD20 in hairy cells. Alteration by low molecular weight B cell growth factor and IFN-alpha. *J. Immunol.* 146:870–878.
18. Goding, J. W. 1980. Structural studies of murine lymphocyte surface IgD. *J. Immunol.* 124:2082–2088.
19. Golay, J. T., and D. H. Crawford. 1987. Pathways of human B-lymphocyte activation blocked by B-cell specific monoclonal antibodies. *Immunology.* 62:279–284.
20. Golay, J. T., E. A. Clark, and P. C. Beverley. 1985. The CD20 (Bp35) antigen is involved in activation of B cells from the G_o to the G_1 phase. *J. Immunol.* 135:3795–3801.
21. Grynkiewicz, G., M. Poenie, and R. Y. Tsien. 1985. A new generation of Ca^{++} indicators with greatly improved fluorescence properties. *J. Biol. Chem.* 260:3440–3450.
22. Hagiwara, S., and H. Ohmori. 1982. Studies of calcium channels in rat clonal pituitary cells with patch electrode voltage clamp. *J. Physiol. (Lond.).* 331:231–252.
23. Hamill, O. P., A. Marty, E. Neher, B. Sakmann, and F. J. Sigworth. 1981. Improved patch clamp techniques for high resolution current recordings from cells and cell-free membrane patches. *Pluegers Arch.* 391:85–110.
24. Hoth, M., and R. Penner. 1992. Depletion of intracellular calcium stores activates a calcium current in mast cells. *Nature (Lond.).* 355:353–356.
25. Hupp, K., D. Siwarski, B. A. Mock, and J.-P. Kinet. 1989. Gene mapping of the three subunits of the high affinity FcR for IgE to mouse chromosomes 1 and 19. *J. Immunol.* 143:3787–3791.
26. Kansas, G. S., and T. F. Tedder. 1991. Transmembrane signals generated through MHC class II, CD19, CD20, CD39, and CD40 antigens induce LFA-1-dependent and independent adhesion in human B cells through a tyrosine kinase-dependent pathway. *J. Immunol.* 147:4094–4102.
27. Klein, E., H. Ben-Bassat, H. Neumann, P. Ralph, J. Zeuthern, A. Polliack, and F. Vanky. 1976. Properties of the K562 cell line derived from a patient with chronic myeloid leukemia. *Intl. J. of Cancer.* 18:421–431.
28. Kondorosi, E., and J. E. Kay. 1977. The role of calcium in lymphocyte activation by the ionophore A23187 and phytohemagglutinin. *Biochem. Soc. Trans.* 5:967–975.
29. Krafte, D. S., T. P. Snutch, J. P. Leonard, N. Davidson, and H. A. Lester. 1988. Evidence for the involvement of more than one mRNA species in controlling the inactivation process of rat and rabbit brain Na^+ channels expressed in *Xenopus* oocytes. *J. Neurosci.* 8:2859–3868.
30. Krueger, B. K. 1989. Toward an understanding of structure and function of ion channels. *FASEB (Fed. Am. Soc. Exp. Biol.) J.* 3:1906–1914.
31. Lambert, J. M., P. D. Senter, A. Yau-Young, W. A. Blattler and V. S. Goldmacher. 1985 Purified immunotoxins that are reactive with human lymphoid cells. *J. Biol. Chem.* 260:12035–12041.
32. Lindau, M., and J. M. Fernandez. 1986. IgE-mediated degranulation of mast cells does not require opening ion channels. *Nature (Lond.).* 319: 150–153.
33. Nadler, L. M., S. J. Korsmeyer, K. C. Anderson, A. W. Boyd, B. Slaughenhoupt, E. Park, J. Jensen, F. Coral, R. J. Mayer, S. E. Sallan, J. Ritz, and S. F. Schlossman. 1984. B cell origin of non-T cell acute lymphoblastic leukemia. A model for discrete stages of neoplastic and normal pre-B cell differentiation. *J. Clin. Invest.* 74:332–340.
34. Noda, M., T. Ikeda, H. Suzuki, H. Takeshima, T. Takahashi, M. Kuno, and S. Numa. 1986. Expression of functional sodium channels from cloned cDNA. *Nature (Lond.).* 322:826–828.
35. Oettgen, H. C., P. J. Bayard, W. Van Ewijk, L. M. Nadler, and C. P. Terhorst. 1983. Further biochemical studies of the human B-cell antigens B1 and B2. *Hybridoma.* 2:17–28.
36. Olsen, R. W., and A. J. Tobin. 1990. Molecular biology of GABAa receptors. *FASEB (Fed. Am. Soc. Exp. Biol.) J.* 4:1469–1480.
37. Ran, S., and B. Rivnay. 1988. Activation of rat basophilic leukemia cells. Temporal identification of the signal calcium influx mediated by the receptor-operated channel pathway. *Eur. J. Biochem.* 171:693–701.
38. Rosenthal, P., I. J. Rimm, T. Umiel, J. D. Griffin, R. Osathanondh, S. F. Schlossman, and E. L. Reinherz. 1983. Ontogeny of human hematopoietic cells: Analysis using monoclonal antibodies. *J. Immunol.* 131: 232–237.
39. Scatchard, G. 1949. The attractions of proteins for small molecules and ions. *Ann. N.Y. Acad. Sci.* 51:660–672.
40. Smeland, E., T. Godal, E. Rudd, K. Beiske, S. Funderud, E. A. Clark, S. Pfeifer-Ohlsson, and R. Ohlsson. 1985. The specific induction of myc protooncogene expression in normal human B cells is not a sufficient event for acquisition of competence to proliferate. *Proc. Natl. Acad. Sci. USA.* 82:6255–6259.
41. Sommer, B., and P. H. Seeburg. 1992. Glutamate receptor channels: novel properties and new clones. *Trends Pharm. Sci.* 13:291–296.
42. Stamenkovic, I., and B. Seed. 1988. Analysis of two cDNA clones encoding the B lymphocyte antigen CD20 (B1, Bp35), a type III integral membrane protein. *J. Exp. Med.* 167:1975–1980.
43. Stashenko, P., L. M. Nadler, R. Hardy, and S. F. Schlossman. 1980. Characterization of a human B lymphocyte-specific antigen. *J. Immunol.* 125:1678–1685.
44. Stashenko, P., L. M. Nadler, R. Hardy, and S. F. Schlossman. 1981. Expression of cell surface markers after human B lymphocyte activation. *Proc. Natl. Acad. Sci. USA.* 78:3848–3852.
45. Stevens, C. F. 1987. Channel families in the brain. *Nature (Lond.).* 328:198–199.
46. Tanabe, T., K. G. Beam, J. A. Powell, and S. Numa. 1988. Restoration of excitation contraction coupling and slow Ca^{++} current in dysgenic muscle by dihydropyridine receptor complementary DNA. *Nature (Lond.).* 336:134–138.
47. Tedder, T. F., and S. F. Schlossman. 1988. Phosphorylation of the B1 (CD20) cell surface molecule expressed by normal and malignant human B lymphocytes. *J. Biol. Chem.* 263:10009–10015.
48. Tedder, T. F., and A. Penta. 1989. Structure of the CD20 antigen and gene of human and mouse B-cells: use of transfected cell lines to examine the workshop panel of antibodies. *In* Leukocyte Typing IV. White Cell Differentiation Antigens. Knapp, W., B. Dorken, W. R. Gilks, E. P. Rieber, R. E. Schmidt, H. Stein, and A. E. G. K. von dem Borne, editors. Oxford University Press, Oxford, U.K. 48–50.
49. Tedder, T. F., L. T. Clement, and M. D. Cooper. 1984. Expression of C3d receptors during human B cell differentiation: Immunofluorescence analysis with the HB-5 monoclonal antibody. *J. Immunol.* 133:678–683.
50. Tedder, T. F., A. W. Boyd, A. S. Freedman, L. M. Nadler, and S. F. Schlossman. 1985. The B cell surface molecule B1 is functionally linked with B cell activation and differentiation. *J. Immunol.* 135:973–979.
51. Tedder, T. F., A. Forsgren, A. W. Boyd, L. M. Nadler, and S. F. Schlossman. 1986. Antibodies reactive with the B1 molecule inhibit cell cycle progression but not activation of human B lymphocytes. *Eur. J. Immunol.* 16:881–887.
52. Tedder, T. F., G. Klejman, C. M. Disteche, D. A. Adler, S. F. Schlossman, and H. Saito. 1988. Cloning of complementary DNA encoding a new mouse B lymphocyte differentiation antigen, homologous to the human B1 (CD20) antigen and localization of the gene to chromosome 19. *J. Immunol.* 141:4388–4394.
53. Tedder, T. F., G. McIntyre, and S. F. Schlossman. 1988. Heterogeneity in the B1 (CD20) cell surface molecule expressed by human B lymphocytes. *Mol. Immunol.* 25:1321–1330.
54. Tedder, T. F., M. Streuli, S. F. Schlossman, and H. Saito. 1988. Isolation and structure of a cDNA encoding the B1 (CD20) cell-surface antigen of human B lymphocytes. *Proc. Natl. Acad. Sci. USA.* 85:208–212.
55. Tedder, T., C. Disteche, E. Louie, D. Adler, C. Croce, S. Schlossman, and H. Saito. 1989. The gene that encodes the human CD20 (B1) differentiation antigen is located on chromosome 11 near the t(11;14) (q13;q32) translocation site. *J. Immunol.* 142:2555–2559.
56. Tsien, R. Y., T. Pozzan, and T. J. Rink. 1982. T-cell mitogens cause early changes in cytoplasmic free Ca^{++} and membrane potential in lymphocytes. *Nature (Lond.).* 295:68–71.
57. Valentine, M. A., T. Cotner, L. Gaur, R. Torres, and E. A. Clark. 1987. Expression of the human B cell surface protein CD20: alteration by phorbol 12-myristate 12-acetate. *Proc. Natl. Acad. Sci. USA.* 84:8085–8089.
58. White, J. R., T. Ishizaka, K. Ishizaka, and R. I. Shaafi. 1984. Direct demonstration of increased intracellular concentration of free calcium as measured by quin-2 in stimulated rat peritoneal mast cell. *Proc. Natl. Acad. Sci. USA.* 81:3978–3982.
59. Worrell, R. T., A. G. Butt, W. H. Cliff, and R. A. Frizzell. 1989. A volume-sensitive chloride conductance in human colonic cell line T84. *Am. J. Physiol. (Cell Physiol.).* 25:C1111–C1119.
60. Zimmer, D. B., C. R. Green, W. H. Evans, and N. B. Gilula. 1987. Topological analysis of the major protein in isolated intact rat liver gap junctions and gap junction-derived single membrane structures. *J. Biol. Chem.* 262:7751–7763.